

# SANS investigation of supramolecular assemblies constructed in aqueous alkyldimethylamine oxide solutions with organic additives

Toyoko Imae

*Department of Chemistry, Faculty of Science, Nagoya University, Nagoya 464, Japan*

Received 6 September 1995; accepted 28 October 1995

## Abstract

SANS investigations were carried out for supramolecular assemblies constructed in aqueous alkyldimethylamine oxide ( $C_n$ DAO) solutions with organic additives. The SANS intensities of aqueous  $C_{12}$ DAO solutions mixed with sodium dodecyl sulfate (SDS) were analyzed on the basis of the rescaled mean spherical approximation. The aggregation numbers and axial ratios of prolate ellipsoidal micelles were maximum at equimolar mixing. Similar behavior was also observed for the pH of the solutions. This non-ideality is caused by the ion-pair formation between protonated  $C_{12}$ DAO and anionic SDS. The electrostatic repulsive interaction was dominant in solutions without salt rather than in solutions with 50 mM NaCl.

The structure of supramolecular assemblies consisting of  $C_{12}$ DAO changed drastically with the addition of cinnamic acid. Vesicles were formed at a mixing molar fraction  $X$  ( $= [\text{cinnamic acid}]/([\text{cinnamic acid}] + [C_n\text{DAO}])$ ) above 0.3. While  $C_{16}$ DAO were associated into a lamellar structure in water, those mixed with cinnamic acid at  $X = 0.17$  formed rodlike micelles which had a cross-sectional radius consistent with the molecular length. Vesicles were also constructed above  $X = 0.3$ . The bilayer thickness of  $C_n$ DAO vesicles and the  $C_{16}$ DAO lamellar structure, evaluated from quantitative analyses of SANS data, was thinner than that estimated from the molecular length. The molecular arrangement in bilayers was estimated.

In the  $L_1$  phase, where the hexanol content is lowest in the  $C_{12}$ DAO/hexanol/water ternary system, globular particles were constructed. The analysis including the contribution of polydispersity was applied for the SANS data. The particle concentration distribution as a function of particle size displayed a bimodal profile, indicating the coexistence of small micelles and microemulsions.

**Keywords:** Alkyldimethylamine oxide; Cinnamic acid; Lamellar layer; Micelle; Small-angle neutron scattering; Sodium dodecyl sulfate; Vesicle

## 1. Introduction

Surfactant molecules in a medium self-associate into various shapes of supramolecular assemblies like micelles, vesicles, emulsions, fibres and liquid crystals, depending on the nature of hydrophilic head group, alkyl chain lengths, surfactant concentration, temperature, salts and salt concentration. When different kinds of surfactant components, cosurfactants, and/or oils are added, the supramo-

lecular assemblies constructed in aqueous surfactant solutions also change their structures and properties, and sometimes the solutions undergo phase transitions.

Multicomponent systems are important in many practical applications, such as detergents, cosmetics, oil recovery, drug delivery systems, emulsified polymerization, photochemistry reactions, coating technology, etc. [1–3]. Therefore, many workers have investigated multicomponent systems using

various techniques, including conductivity, fluorescence spectroscopy, voltammetry, rheology, NMR, light scattering, small-angle X-ray scattering (SAXS), small-angle neutron scattering (SANS), and electron microscopy [4–16]. Having determined phenomenologically and physicochemically the characterization of multicomponent systems, the approach based on the nature of components and the geometric model of microscopic structure become important [17].

SANS is a suitable technique for studying microscopic structures of molecular assemblies and the interactions between them. So far, SANS investigations have been carried out for various kinds of supramolecular systems [18–33] in order to determine their sizes and shapes. The effect of polydispersity has also been discussed [34,35]. Moreover, a theoretical analysis of the intraparticle and interparticle interference effects has been applied to small micelles [18–20,22,25,26,36].

It is known that weak-base surfactants, alkyldimethylamine oxide ( $C_n$ DAO), can form many molecular assemblies in water depending on the conditions, and their solution behavior has been extensively investigated [37–45]. This paper reviews the SANS investigations of the multicomponent systems of  $C_n$ DAO with water and additives, namely sodium dodecyl sulfate (SDS), cinnamic acid, or hexanol. The SANS data are analyzed on a theoretical basis [46–47] and the microscopic structures of molecular assemblies are discussed in relation to their properties.

## 2. Analytical

### 2.1. SANS intensity

Supposing a disordered system, namely, an isotropic ensemble of identical particles, the SANS intensity  $I(Q)$  as a function of the Bragg wave number  $Q$  is written as [46–48]

$$I(Q) = n_p [\langle F(Q) \rangle_{\theta'}^2 S(Q) + \langle |F(Q)|^2 \rangle_{\theta'} - \langle F(Q) \rangle_{\theta'}^2], \quad (1)$$

where  $n_p$  is the number density of colloidal particles.  $F(Q)$  and  $S(Q)$  are the particle form factor

and the interparticle structure factor, respectively, and  $\theta'$  is the angle between the major axis and the Bragg wave vector. The particle form factor for nonspherical particles must be averaged over all  $\theta'$  values.

The interparticle structure factor is related to the interparticle interaction potential  $V(r)$  through the radial distribution function  $g(r)$ . If the interparticle structure factor is Fourier-transformed, then

$$g(r) = 1 + (1/12\pi\eta r) \int_0^{\infty} [S(Q) - 1] Q r \sin Qr \, dQ, \quad (2)$$

where  $\eta$  ( $= \pi n_p R^3/6$ ) is the volume fraction of spherical particles of finite radius  $R$ , and  $r$  is the center-to-center distance between particles. On the basis of the theory of simple liquids [49], an Ornstein–Zernike equation is described by

$$g(r) - 1 = h(r) = c(r) + n_p R^3 \int h(|r - r'|) c(r') \, dr' \\ c(r) = -V(r)/k_B T \quad r > R, \\ h(r) = -1 \quad r \leq R, \quad (3)$$

where  $k_B$  is Boltzmann's constant, and  $T$  is the absolute temperature.  $h(r)$  is the total correlation function and  $c(r)$  is the direct correlation function.

Eq. (1) can be written as

$$I(Q) = n_p \langle |F(Q)|^2 \rangle_{\theta'} \equiv n_p P(Q) \quad (4)$$

for a dilute solution, because the interparticle scattering factor approaches unity.  $P(Q)$  is the intraparticle structure factor, which depends on the particle geometry.

### 2.2. Intraparticle structure factor

#### 2.2.1. Ellipsoidal and spherical particles

For a monodisperse system of prolate ellipsoidal particles with semimajor and semiminor axes,  $a$  and  $b$ , the intraparticle structure factor is written

as

$$P(Q) = V^2(\rho - \rho_s)^2 \left| \int_0^1 (3j_1(u)/u) d \cos \theta' \right|^2,$$

$$u = Q[a^2 \cos^2 \theta' + b^2(1 - \cos^2 \theta')]^{1/2},$$

$$V = 4\pi ab^2/3 \quad \text{for prolate ellipsoids,}$$

$$u = Q[a^2(1 - \cos^2 \theta') + b^2 \cos^2 \theta']^{1/2},$$

$$V = 4\pi a^2 b/3 \quad \text{for oblate ellipsoids,} \quad (5)$$

where  $V$  is the total volume of a particle.  $\rho$  and  $\rho_s$  are the mean coherent neutron scattering length densities of the particle and the solvent, respectively.  $j_1(x)$  is the first-order spherical Bessel function, which is given by

$$j_1(x) = (\sin x - x \cos x)/x^2,$$

$$3j_1(x)/x = 1 \quad \text{at } x \rightarrow 0. \quad (6)$$

The intraparticle structure factor for homogeneous spherical particles of radius  $R$  is described as follows:

$$P(Q) = V^2(\rho - \rho_s)^2 [3j_1(QR)/QR]^2,$$

$$V = 4\pi R^3/3. \quad (7)$$

When  $R_G$  is the radius of gyration,  $J_1(u)$  is developed by a small  $u$  value, if the  $QR_G$  value is small. Then

$$P(Q) = V^2(\rho - \rho_s)^2 \exp(-R_G^2 Q^2/3),$$

$$R_G^2 = (a^2 + 2b^2)/5 \quad \text{for prolate ellipsoids,}$$

$$R_G^2 = (2a^2 + b^2)/5 \quad \text{for oblate ellipsoids,}$$

$$R_G^2 = 3R^2/5 \quad \text{for spheres.} \quad (8)$$

This is known as a Guinier equation. From Eq. (8) we can see that logarithmic  $P(Q)$  values decrease linearly with increasing  $Q^2$ .

### 2.2.2. Rigid rod and plane disk particles

If particles have a cylindrical structure of length  $L$  and radius of the transversal cross-section  $R_t$  such that  $L \gg R_t$ , the SANS intensity is described

by

$$QP(Q) = \pi V A_t (\rho - \rho_s)^2 [2j_1(QR_t)/QR_t]^2,$$

$$V = L A_t = \pi R_t^2 L, \quad (9)$$

for large  $QL$  values.  $A_t$  is an area of the transversal cross-section of the rod.

When  $QR_{G,C}$  value is not large,

$$QP(Q) = \pi V A_t (\rho - \rho_s)^2 \exp(-R_{G,C}^2 Q^2/2),$$

$$R_{G,C} = R_t/\sqrt{2}, \quad (10)$$

where  $R_{G,C}$  is the radius of gyration for the transversal cross-section. Then a plot of  $\log QP(Q)$  against  $Q^2$  displays a linear decrease.

For disk of radius  $R$  and thickness  $t$  such that  $R \gg t$ ,

$$Q^2 P(Q) = 2\pi(V^2/A_t)(\rho - \rho_s)^2 [\sin(Qt/2)/(Qt/2)]^2,$$

$$V = t A_t = \pi R^2 t, \quad (11)$$

and

$$Q^2 P(Q) = 2\pi(V^2/A_t)(\rho - \rho_s)^2 \exp(-R_{G,C}^2 Q^2),$$

$$R_{G,C} = t/\sqrt{12}, \quad (12)$$

for small  $QR_{G,C}$  values.  $V$  and  $A_t$  are the volume and the area of the disk, respectively.  $R_{G,C}$  is the radius of gyration of the thickness.

### 2.2.3. Vesicles

Suppose that vesicles have a unilamellar spherical shell of inner and outer radii  $R_i$  and  $R_o$ . The intraparticle structure factor is

$$P(Q) = (\rho - \rho_s)^2$$

$$\times [3V_o j_1(QR_o)/QR_o - 3V_i j_1(QR_i)/QR_i]^2,$$

$$V_i = 4\pi R_i^3/3, \quad V_o = 4\pi R_o^3/3, \quad (13)$$

where  $V_i$  and  $V_o$  are the volumes of spheres with radii  $R_i$  and  $R_o$ , respectively.

In the large  $QR_G$  region, where  $R_G^2 = 3(R_o^5 - R_i^5)/5(R_o^3 - R_i^3)$  for a spherical shell,

$$Q^2 P(Q) = 2\pi(A/V)(\rho - \rho_s)^2 (R_o - R_i)^2,$$

$$V = V_o - V_i, \quad A = 4\pi(R_o^2 + R_i^2). \quad (14)$$

It should be noted that the  $Q^2 P(Q)$  values are independent of  $Q^2$ .

### 2.2.4. Lamellar layers

For a periodic multilamellar structure with infinitely extended bilayers [50],

$$Q^2 P(Q) = (2\pi/n_p)(t^2/D)(\rho - \rho_s)^2 [\sin(Qt/2)/(Qt/2)]^2, \\ D = t'/\phi = 2\pi/Q_{\max}, \quad (15)$$

where  $t$  is the width of the scattering length density profile.  $D$  is the repeat distance of the bilayers and is calculated from the first-order Bragg peak position at  $Q_{\max}$ , using the relation described in Eq. (15).  $t'$  is the bilayer thickness, that is, the width of the mass-density profile, so that  $t' \geq t$ .  $\phi$  denotes the volume fraction of the component molecules.

For small  $QR_{G,c}$ ,

$$Q^2 P(Q) = (2\pi/n_p)(t^2/D)(\rho - \rho_s)^2 \exp(-R_{G,c}^2 Q^2), \\ R_{G,c} = t/\sqrt{12}. \quad (16)$$

$R_{G,c}$  is the radius of gyration of the thickness  $t$ . Eq. (16) indicates a linear relationship between  $\log Q^2 P(Q)$  and  $Q^2$ .

## 3. Experimental

The SANS measurements were made using the cold neutron small-angle scattering instrument SAN and WINK at the National Laboratory for High Energy Physics (KEK). The instrument was operated at a neutron radiation of 1–16 Å wavelength at room temperature ( $\sim 25^\circ\text{C}$ ). The SANS intensities were obtained as a function of  $Q$  ( $= (4\pi/\lambda) \sin(\theta/2)$ ), where  $\lambda$  is the neutron radiation wavelength and  $\theta$  is the scattering angle. A rectangular quartz cell of dimensions  $22 \times 40 \times 2$  mm was used.  $\text{D}_2\text{O}$  was utilized as a solvent for the SANS measurements.

## 4. Results and discussion

### 4.1. Mixed micelles of dodecyltrimethylamine oxide and sodium dodecyl sulfate

When ionic surfactants are added to aqueous solutions of the nonionic surfactant,  $\text{C}_n\text{DAO}$ , the

mixed solutions sometimes display non-ideal behavior: the pH of mixed solutions with anionic surfactant, SDS, displayed a maximum, while the pH of mixed solutions with a cationic surfactant, alkyltrimethylammonium bromide ( $\text{C}_n\text{TAB}$ ), was additive [51]. The critical micelle concentration (CMC) and the partial molar volume as a function of the mixed micelle composition exhibited a negative deviation from ideal behavior, although the heat capacity behaved ideally [52]. The rheological behavior of solutions also changed drastically [51,53]. We suggest that these phenomena are the results of specific interactions between heterogeneous surfactants and are related to the micellar aggregation and the intermicellar interactions.

SANS measurements were performed on mixed solutions of  $\text{C}_{12}\text{DAO}$  and SDS at a total surfactant concentration of 80 mM in  $\text{D}_2\text{O}$  with and without 50 mM NaCl. The SANS results were obtained for solutions of different mixing molar fractions  $X$  ( $= [\text{SDS}]/\{[\text{SDS}] + [\text{C}_{12}\text{DAO}]\}$ ). As seen in Fig. 1, there was a peak around  $Q \sim 0.03 \text{ \AA}^{-1}$  for solutions of  $X = 0$ . In the absence of NaCl, the peak shifted to larger  $Q$  values with increasing  $X$ , whereas the peak scattering intensity was highest at  $X = 0.4$ . For systems with 50 mM NaCl, the scattering intensity decreased monotonically with increasing  $Q$  values at  $X = 0.1$ – $0.5$  and had a peak at  $X > 0.5$ .

The SANS intensities did not display peaks for aqueous solutions of  $\text{C}_{14}\text{DAO}$  [33] and oligooxyethylene alkyl ethers ( $\text{C}_n\text{E}_m$ ) [20,22] at dilute concentrations. In contrast, aqueous  $\text{C}_n\text{E}_m$  solutions at high concentrations had a peak in the SANS curve [20,26,30], as did an aqueous  $\text{C}_{12}\text{DAO}$  solution ( $X = 0$ ) of 80 mM. Scattering angle dependence similar to the latter SANS behavior was reported in light scattering for aqueous solutions of  $\text{C}_n\text{DAO}$  and oleyldimethylamine oxide [38,44].

SANS profiles with remarkable peaks are a more common feature of aqueous solutions of ionic surfactants such as SDS at finite micellar concentrations [18,22,24,25,27,28,34,35]. The intermicellar interactions in aqueous 0.1 M  $\text{C}_{16}\text{TAB}$  solutions disappeared due to electrostatic shielding when 0.2 M KCl was added [32]. The electrostatic shielding occurred with the addition of 50 mM NaCl only in mixed solutions of  $\text{C}_{12}\text{DAO}$  and

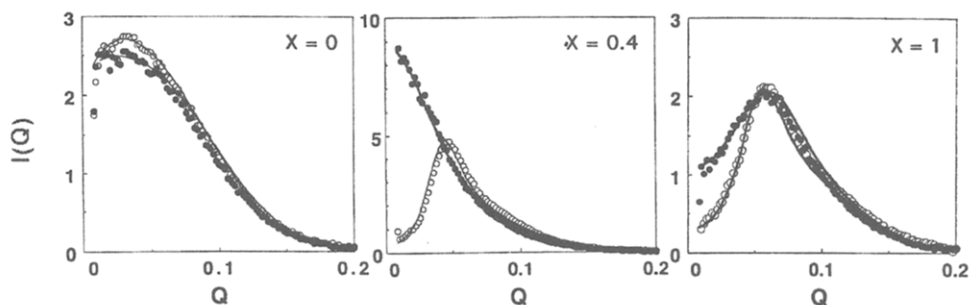


Fig. 1. SANS data from mixed solutions of  $C_{12}$ DAO and SDS at different mixing molar fractions. Total surfactant concentration is 80 mM. NaCl concentrations:  $\circ$  0 mM;  $\bullet$  50 mM. The solid lines are the calculated curves.

SDS at  $X = 0.1$ – $0.5$ , because mixed micelles composed of ionic and nonionic surfactants have less charge to be shielded than those of pure ionic surfactant micelles.

The intraparticle structure factor for ellipsoidal particles can be applied for small mixed micelles of  $C_{12}$ DAO and SDS. Suppose that the ellipsoidal structure is composed of a hydrophobic inner core with semimajor and semiminor axes  $a$  and  $b$ , respectively, and a surrounding hydrophilic shell with thickness  $d$  including hydrated  $D_2O$  [19]. Then Eq. (5) for a prolate ellipsoid is rewritten as

$$P(Q) = \int_0^1 [V_M(\rho_a - \rho_s)(3J_1(U_m)/u_m) + V_i(\rho_i - \rho_a)(3J_1(u_c)/u_c)]^2 d \cos \theta',$$

$$u_m = Q[(a + d)^2 \cos^2 \theta' + (b + d)^2(1 - \cos^2 \theta')]^{1/2},$$

$$u_c = Q[a^2 \cos^2 \theta' + b^2(1 - \cos^2 \theta')]^{1/2},$$

$$V_i = 4\pi ab^2/3,$$

$$V_M = 4\pi(a + d)(b + d)^2/3, \quad (17)$$

where  $\rho_i$  and  $\rho_a$  are the mean coherent neutron scattering length densities of the core and shell, respectively.  $V_i$  and  $V_M$  are the volumes of the core and ellipsoid, respectively.

If  $v_{sf}$ ,  $v_{hc}$ , and  $v_{hg}$  represent the volumes of surfactant, hydrocarbon chain, and polar head,

respectively, the following relations are described:

$$v_{sf} = v_{hc} + v_{hg},$$

$$V_i = mv_{hc},$$

$$V_M = mv_{hc} + mv_{hg} + ymv_s, \quad (18)$$

where  $m$  is the aggregation number,  $y$  is the number of hydrated  $D_2O$  molecules per surfactant, and  $v_s$  is the volume of  $D_2O$ . Supposing that the head group assumes a spherical shape with diameter  $d$  equal to the thickness of the ellipsoidal shell, the volume  $v_{hg}$  can be calculated. The volume  $v_{hc}$  was calculated using Tanford's equation [54].

There was an apparent contribution from interparticle interactions in the mixed solutions examined here, except those at  $X = 0.1$ – $0.5$  for a system with 50 mM NaCl. The interaction between micelles in the mixed solutions is mainly due to a Coulomb repulsive force. This was indicated by the fact that the electrophoretic mobility was negative for solutions at all mixing ratios in the presence of 50 mM NaCl [55]. The van der Waals attractive interaction, which is another kind of important interaction, is weaker than the electrostatic interaction so that it is negligible in this case.

The electrostatic repulsive potential between two identical spherical macro-ions of finite diameter  $R$  with hard core is described by [56]

$$V(r) = \pi\epsilon_0\epsilon R^2\psi_0^2 \exp[-\kappa(r - R)]/r \quad r > R,$$

$$V(r) = \infty \quad r \leq R,$$

$$\psi_0 = z_m/\pi\epsilon_0\epsilon R(2 + \kappa R), \quad (19)$$

if  $\kappa R < 6$ . Here  $\epsilon_0$  is the permittivity of free space,  $\epsilon$  is the dielectric constant of solvent medium, and  $\kappa$  is the Debye–Hückel inverse screening length.  $\psi_0$  is the surface potential, and  $z_m$  is the electric charge of the macro-ion.

The treatment for the interparticle structure factor by Hansen and Hayter [36] can then be applied to the solutions in the present work. The treatment, called rescaled mean spherical approximation (RMSA), is an expansion to dilute ( $\eta < 0.2$ ) solutions of the mean spherical approximation (MSA) introduced by Hayter and Penfold [19]. There, a diameter  $R$  of spherical macro-ions is replaced by a diameter  $R'$  determined by a Gillan criterion, as follows:

$$g^{\text{RMSA}}(r = R') = 0, \quad \text{with } s = R/R', \quad (20)$$

where  $s$  is a rescaled factor. The conditions  $\eta < 0.2$  and  $\kappa R < 6$  are satisfied in the systems examined here.

Using available values of parameters such as critical micelle concentration and  $v_{\text{sf}}$  [52], the calculated SANS intensities were fitted to the observed ones on the basis of analytical equations, assuming an ellipsoidal structure and RMSA with a diameter equivalent to a prolate ellipsoid. The solid lines in Fig. 1 show the results of this fitting. An optimum set of unknown fitting parameters, semiminor axis  $b$  of the ellipsoidal core, the axial ratio  $a/b$ , the average electric charge number  $z_m/em$  ( $e$  is the elementary electric charge) per surfactant, and the rescaled factor  $s$  was determined from the fitting. Then other parameters (diameter  $R$ , aggregation number  $m$  of a micelle, volume fraction  $\eta$ , and number  $y$  of hydrated  $\text{D}_2\text{O}$  per surfactant) were calculated. The numerical values of some of these parameters are listed in Table 1.

The prolate ellipsoidal structure was preferable to the oblate ellipsoidal structure. The semiminor axis  $b = 18\text{--}19 \text{ \AA}$  of prolate ellipsoid was consistent with the calculated alkyl chain length. While  $\text{C}_{12}\text{DAO}$  or SDS micelles had axial ratios as small as 1.3–1.4, prolate ellipsoidal micelles with axial ratios of 1.5–4.5 were formed in the mixed solutions. As seen in Fig. 2, the obtained aggregation number of mixed micelles did not display additivity but had a maximum at equimolar mixing in relation to the variation of the axial ratios, suggesting

the formation of ellipsoidal or very short rodlike micelles, while the  $\text{D}_2\text{O}$  hydration was minimum. Maximum values of the axial ratio and the aggregation number were dominant in the presence of 50 mM NaCl rather than in the absence of NaCl, owing to the salting-out effect.

As shown in Fig. 2, there was also anomalous behavior in the pH changes of the solutions: the pH became very high (pH = 10–11.5) compared with that of SDS or  $\text{C}_{12}\text{DAO}$  (pH = 7–9). On the other hand, it is apparent from Fig. 3 that the average electric charge numbers  $z_m/em$  per surfactant in micelles increased with an increase in the molar fraction of SDS, as expected, indicating the charge number of 0.13–0.15 per SDS in micelles or the counter-ion binding of 0.85–0.87 per SDS. The numerical values were close to those obtained from  $\text{Na}^+$  potentiometric titrations [55], the evaluations by Hayter and Penfold [19] and Bendedouch and Chen [25], and the calculation by Hayter [57] on the basis of the dressed micelle model. This means that the interaction between mixed micelles is mainly that of an electrostatic repulsion force between charged micelles.

A self-protonated  $\text{C}_{12}\text{DAO}$  molecule interacts electrostatically with an SDS molecule to form an ion-pair, as illustrated in Fig. 4, inducing the non-ideal behavior in the solution pH and the micelle aggregation number. Ion-paired surfactants behave like hydrophobic double-tailed surfactants, promoting the formation of micelles with larger aggregation numbers. The release of hydroxyl ions caused by the self-protonation of  $\text{C}_{12}\text{DAO}$  allows the solution pH to increase. The addition of NaCl shields the electric charge of micelles and the electrostatic interaction, resulting in the disturbance of the ion-pairing between surfactants and the electrostatic repulsive interaction between micelles.

The non-ideal behavior of the micelle aggregation number as a function of the mixing fraction can be compared with the behavior as a function of the degree of ionization [37]. The aggregation numbers for aqueous  $\text{C}_{12}\text{DAO}$  solutions were maximum when the degree of ionization was  $\sim 0.5$ . This suggests the possible ion-pairing between nonprotonated and protonated  $\text{C}_{12}\text{DAO}$  in the

Table 1

Parameters obtained from SANS analysis for mixtures of C<sub>12</sub>DAO and SDS in water and in 50 mM NaCl

X	d (Å)	In water					In 50 mM NaCl				
		b (Å)	a/b	m	y	z <sub>m</sub> /em	b (Å)	a/b	m	y	z <sub>m</sub> /em
0	4.86	18.5	1.45	110	8.2	0.015	18.5	1.3	98	8.7	0.04
0.1	4.82	18.5	1.95	148	7.3	0.06	18.0	1.9	144	6.0	
0.2	4.77	18.5	2.30	174	6.9	0.08	18.5	4.0	302	6.1	
0.3	4.73	18.5	2.37	179	6.9	0.079	19.0	4.0	328	5.8	
0.4	4.69	18.5	2.58	195	6.7	0.075	18.0	4.0	279	6.2	
0.5	4.65						19.0	4.0	328	5.7	
0.6	4.60	18.5	2.10	159	6.9	0.080	18.5	4.5	341	5.8	0.06
0.7	4.55	18.5	1.75	133	7.2	0.10	18.5	2.75	208	6.4	0.09
0.8	4.50	18.5	1.50	113	7.8	0.12	18.5	2.1	159	6.8	0.10
1.0	4.41	18.5	1.30	98	8.1	0.14	18.5	1.4	106	7.7	0.13

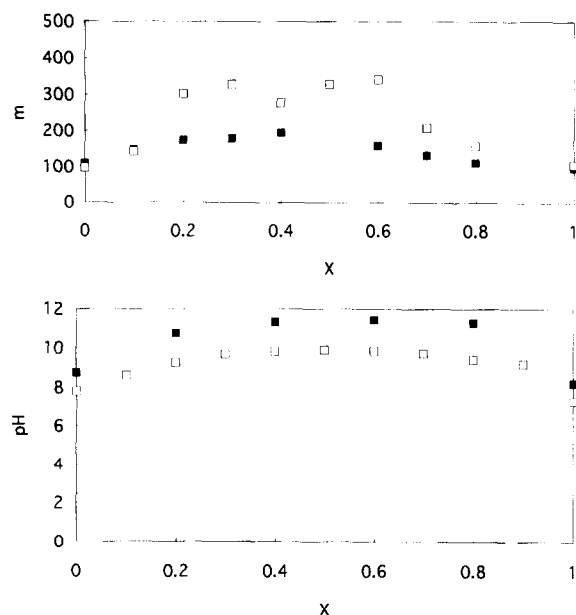


Fig. 2. Micelle aggregation numbers in mixed solutions of C<sub>12</sub>DAO and SDS and solution pH as a function of mixing molar fraction. Total surfactant concentration is 80 mM. NaCl concentrations: ■ 0 mM; □ 50 mM.

moderately titrated C<sub>12</sub>DAO solutions, as well as between C<sub>12</sub>DAO and SDS in the mixed solutions.

The behavior of micellar mass weights and interactions in the mixed solutions of C<sub>12</sub>DAO and SDS is in contrast to that in mixtures of C<sub>n</sub>DAO and C<sub>n</sub>TAB [51,58]. In the latter system, micellar sizes and solution pH changed almost linearly with change in mixing fraction. The difference in the

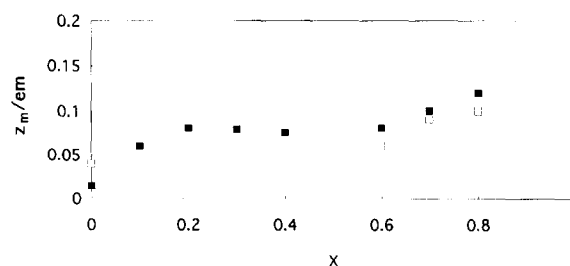


Fig. 3. Average electric charge numbers per surfactant of micelles in mixed solutions of C<sub>12</sub>DAO and SDS as a function of mixing molar fraction. Total surfactant concentration is 80 mM. NaCl concentrations: ■ 0 mM; □ 50 mM.

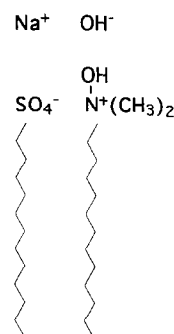


Fig. 4. Schematic representation of ion-pair formation in mixed solutions of C<sub>12</sub>DAO and SDS.

behavior of C<sub>n</sub>DAO–SDS and C<sub>n</sub>DAO–C<sub>n</sub>TAB complexes is due to the formation of different orientations of the amine oxide dipole with sulfate and ammonium ions in the ion-pairing [51].

The number of hydrated D<sub>2</sub>O per surfactant for

pure  $C_{12}$ DAO or SDS micelles was close to that reported for SDS micelles and higher than those for alkyltrimethylammonium halide micelles [19]. Hydrated  $D_2O$  decreased with increasing micelle aggregation number in the mixed solutions of  $C_{12}$ DAO and SDS, although the inverse dependence was reported by Hayter and Penford [19].

Microscopic structures of small molecular assemblies such as ellipsoidal micelles can be clarified by SANS investigations as described above. However, very few SANS investigations have been reported for mixed systems. Structural investigations of mixed micelles by SANS should solve problems related to the miscibility of component molecules. On the other hand, interparticle interactions are intrinsic to dispersions of colloidal particles in a medium. SANS is a unique technique for estimating the total interparticle interaction potential in a solution. This information should be compared with the electrostatic interaction which is calculated from electrophoretic mobility investigations. Moreover, the recent development of surface force measurement by atomic force microscopy and surface force apparatus may bolster the SANS results.

#### 4.2. Vesicles of dodecyltrimethylamine oxide formed in the presence of cinnamic acid

Organic counter-ions and inorganic ions such as chloride, bromide, and iodide affect the molecular self-assembly in different ways. It was reported that the photochemical reaction of aromatic unsaturated carboxylic acids proceeds effectively in molecular assembly matrices such as in dispersions of clays and in solutions of micelles [59–62]. The reactions result in different reaction efficiencies and stereochemical selectivities, depending on the assembly structures [63–65]. Therefore, the optimum matrix where the specific photoreaction occurs most effectively can be determined.

While  $C_{12}$ DAO forms small micelles,  $C_{16}$ DAO constructs lamellar layers in water, as can be seen in Fig. 5 [42,43,66]. Light scattering and transmission electron microscopic (TEM) investigations have verified that the size and macroscopic structure of molecular assemblies change drastically at a mixing molar fraction  $X$  ( $= [\text{cinnamic acid}] /$

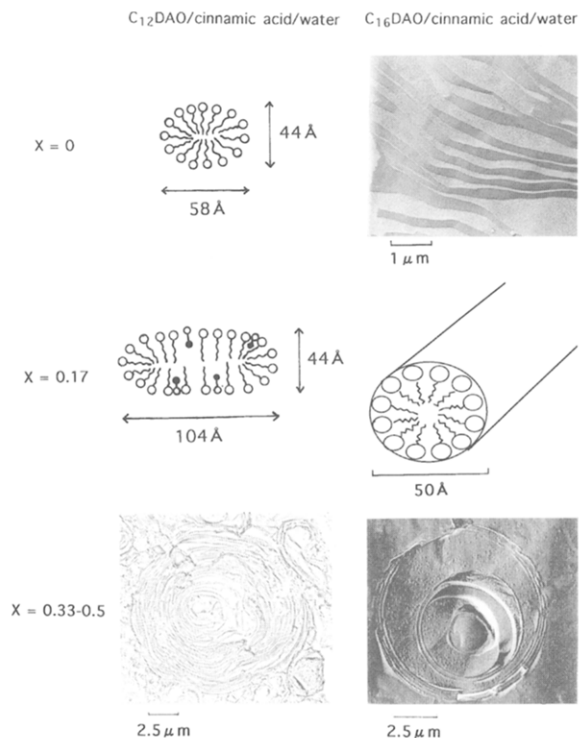


Fig. 5. Molecular assembly formation in mixed solutions of  $C_n$ DAO and cinnamic acid. Photographs were taken by freeze-fracture TEM.

( $[\text{cinnamic acid}] + [C_n\text{DAO}]$ ) of  $\sim 0.29$ , when cinnamic acid was added [67,68]. Vesicular TEM images with multilamellar layers were observed in solutions of higher molar fractions (see Fig. 5).

SANS measurements were carried out on mixed solutions prepared at a constant total concentration of  $C_n$ DAO and cinnamic acid with different mixing fractions. The results are shown in Figs. 6 and 7, where the solid lines are analytical fitting curves as mentioned below. For dilute solutions at a total concentration of  $2 \text{ mg cm}^{-3}$ , since the interparticle structure factor can be approximated to be unity, the intraparticle structure factor contributes to the SANS intensity as a function of Bragg wave number.

##### 4.2.1. $C_{12}$ DAO/cinnamic acid

Small micelles formed in an aqueous  $C_{12}$ DAO solution without cinnamic acid take a prolate ellipsoidal structure as described above (see Fig. 5).

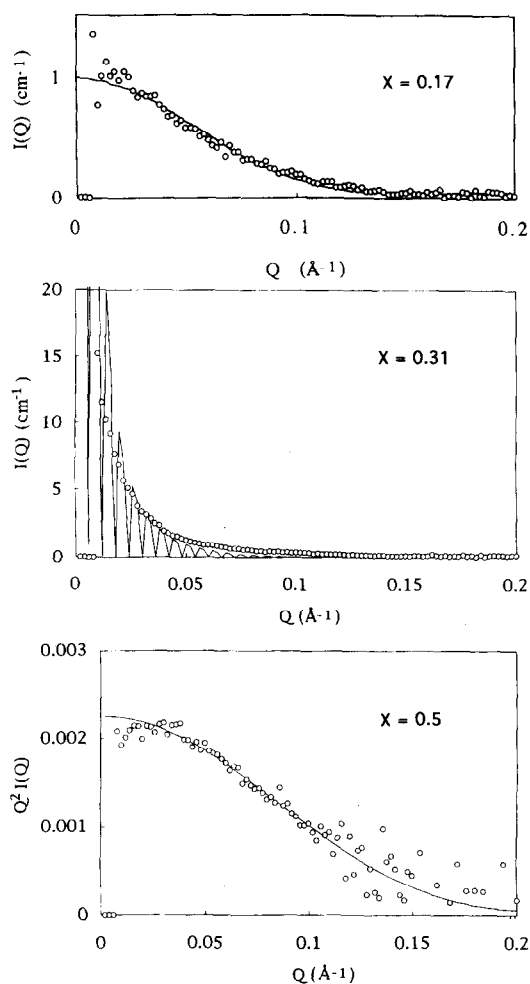


Fig. 6. SANS data for mixed solutions of  $C_{12}$ DAO and cinnamic acid at different mixing fractions. Solid lines represent the calculated curves.

Then the analytical equations (4)–(8) for a monodisperse system were applied for the solution at  $X = 0.17$ . The SANS intensity evaluated using a set of unknown parameters of  $a$ ,  $b$  and  $m$  was fitted to the observed data. The optimum theoretical curve was obtained for prolate ellipsoid with axial ratio of 2.4, as illustrated in Fig. 5. The aggregation number of 101 was in good agreement with that obtained from light scattering [67]. The observed SANS data were not reproduced by the spherical particle model. Those results confirm that a small amount of cinnamic acid acts as a cosurfactant rather than as an oil component to form preferably

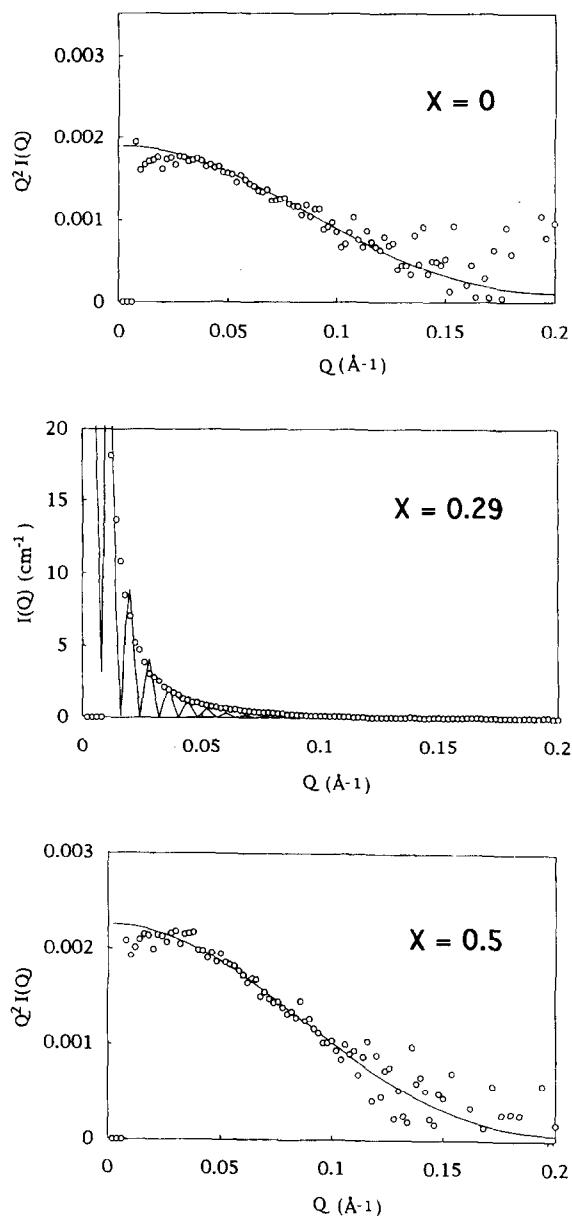


Fig. 7. SANS data for mixed solutions of  $C_{16}$ DAO and cinnamic acid at different mixing fractions. Solid lines represent the calculated curves.

ellipsoidal micelles, but not swollen micelles or microemulsions.

Vesicles of various sizes were observed by TEM in the solution at  $X = 0.29$  [67]. Since the average mass weight of molecular assemblies evaluated from light scattering was only 6 times larger than

that of micelles at  $X = 0$  [67], small micelles and vesicles must coexist in the solution. A numerical analysis for this system was not performed, because the contributions from both micelles and vesicles had to be considered.

Molecular assemblies were vesicles in translucent solutions at  $X = 0.31$ – $0.5$  [67]. Although the quantitative analysis for a system of  $X = 0.31$ , on the basis of Eqs. (4) and (13) for vesicles, was tried under the assumption of vesicles with a unilamellar membrane, the evaluated outer radius did not agree with that from light scattering. The numerical inconsistency comes from the polydispersity in vesicular size and shape, bilayer number, and interbilayer distance.

The SANS data for solutions at  $X = 0.33$ – $0.5$  were consistent with analytical Eqs. (15) and (16) for lamellar layers rather than those for vesicles. The vesicles were too large to obtain information for their whole size of SANS. However, the local lamellar layer thickness and interlamellar distance were obtainable from SANS. Although the bilayer thicknesses of  $23$ – $30$  Å evaluated from the numerical fitting increased with the mixing fraction, as expected from adsorption of cinnamic acid on membranes, the absolute values were less than those estimated from the molecular length.

#### 4.2.2. $C_{16}$ DAO/cinnamic acid

Lamellar layers were formed in a gel-like  $C_{16}$ DAO solution without cinnamic acid [42,43]. Although equations for the lamellar layer structure were applied to this system, the calculated bilayer thickness of  $30$  Å was less than that estimated ( $53$  Å). Tilt or random orientation of alkyl chains may occur in membrane bilayers, as illustrated in Fig. 8.

The viscous, but transparent solution character at  $X = 0.17$  suggests the formation of rodlike micelles (Fig. 5). It is noticed that rodlike micelles are formed in aqueous  $C_{16}$ DAO solutions at temperatures higher than  $30^\circ\text{C}$  [39,41]. As expected, the SANS data fitted analytical Eqs. (9)–(12) for rigid rods but did not satisfy those for ellipsoids, vesicles and lamellar layers. The calculated cross-sectional radius of  $25$  Å was almost consistent with the estimated molecular length.

Vesicles of various sizes with uni- to multilam-

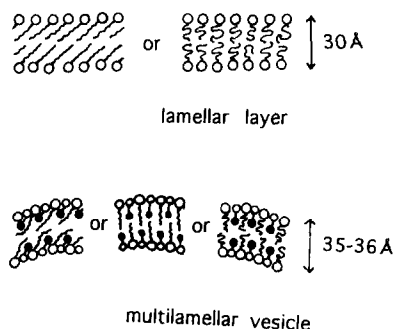


Fig. 8. Schematic representation of possible models for molecular arrangements in  $C_{16}$ DAO lamellar bilayers and  $C_{16}$ DAO/cinnamic acid vesicle membranes.

ellar layers existed in solutions at  $X = 0.29$  and  $0.31$  [67]. Although the observed intensity was compared with values calculated on the basis of analytical equations for vesicles with a unilamellar membrane, the calculated outer radius of the vesicles was not consistent with the light scattering results [67] because the size polydispersity and the bilayer multiplicity of vesicles were not considered in this analysis.

Vesicles formed in solutions at  $X = 0.33$ – $0.5$  were larger and had multilamellar layers [67]. The bilayer thickness of  $35$ – $36$  Å obtained from the theoretical calculation for the lamellar layer model was thinner than the bilayer thickness expected. Similar results were obtained for  $C_{12}$ DAO/cinnamic acid vesicles and for  $C_{16}$ DAO lamellars. The possibility of tilt, random orientation, or comb-shaped arrangement of alkyl chains in membrane bilayers can be suggested, as illustrated in Fig. 8. There was a weak Bragg peak around  $Q = 0.03$  Å<sup>-1</sup> for solutions above  $X = 0.33$ . The distance of  $250$  Å, calculated on the basis of Eq. (15), is assigned to the average interlamellar distance.

#### 4.2.3. Photochemical reaction

SANS can give quantitative information concerning nanometer order, such as the shape of small micelles, the cross-section of rodlike micelles, the lamellar thickness, and the interlamellar distance, as described above. The photo-cyclodimerization of cinnamic acid in aqueous  $C_n$ DAO solutions is expected to be influenced by microscopic structures of molecular assemblies, that is,

the location and organization of cinnamic acid on the reaction matrices. In fact, dimerization was promoted in vesicles rather than in micelles, and anti-head-to-head dimers were found to be produced predominantly more than other isomers [62,67]. These results suggest that photochemical reactions can be controlled by reaction matrices. This will be supported by additional photochemical experiments with the other combinations of molecular assemblies and unsaturated carboxylates.

#### 4.3. $L_1$ phase in dodecyltrimethylamine oxide/hexanol/water ternary system

When an oil component, hexanol, was added to aqueous  $C_{12}$ DAO solutions, several single phases were observed even at dilute concentrations of  $C_{12}$ DAO and hexanol [69]. Each phase was distinguished by characteristic solution properties such as turbidity, iridescence, shear anisotropy and rheology. The characteristic properties of each phase were closely related to the molecular assembly in the solution, which was characterized by TEM [70].

The  $L_1$  phase with lowest hexanol content is transparent, fluid and optically isotropic. The average molecular weight evaluated from light scattering increased with increasing molar fraction of hexanol  $X$  ( $= [\text{hexanol}]/([\text{hexanol}] + [C_{12}\text{DAO}])$ ) and was 13 times larger in a solution at  $X = 0.44$  than in a solution without hexanol [71]. The average hydrodynamic radii of 56 and 98 Å for molecular assemblies in the solutions at  $X = 0.33$  and 0.44, respectively, were larger than the estimated radius for pure  $C_{12}$ DAO micelles. The TEM photograph of a mixture of  $X = 0.29$  (50 mM  $C_{12}$ DAO/20 mM hexanol) in Fig. 9 displays the image of globular particles of 50–400 Å diameter in the  $L_1$  phase, indicating the polydispersity in particle size.

SANS was measured for the  $C_{12}$ DAO/hexanol/water ternary system in the  $L_1$  phase, indicating the polydispersity in particle size.

SANS was measured for the  $C_{12}$ DAO/hexanol/water ternary system in the  $L_1$  phase at  $X = 0, 0.29$ , and 0.44 for 20 and 50 mM  $C_{12}$ DAO. The Guinier plots are shown in Fig. 10. Although

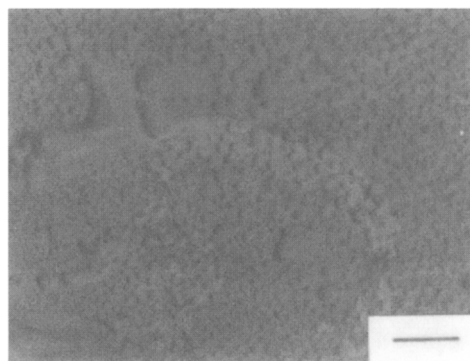


Fig. 9. TEM photograph for 50 mM  $C_{12}$ DAO/20 mM hexanol/water ( $X = 0.29$ ) system. Bar represents 200 nm.

the plot for the aqueous  $C_{12}$ DAO solution without hexanol displayed a linear decrease with  $Q^2$ , those for solutions at  $X = 0.29$  and 0.44 decreased with downward curvature.

Since the particle concentrations examined are low, and the particles are not very large, interparticle interactions are negligible. Therefore, the intraparticle structure factor must contribute to the SANS profiles. The scattering intensity of polydisperse particles is then the sum of the contributions from  $N$ -mer particles with a molar concentration  $C_N$  and radius of gyration  $R_{G,N}$ :

$$I(Q) = \sum_{N=N_0}^{\infty} C_N N (b_m - \rho_s V_m)^2 \exp(-R_{G,N}^2 Q^2/3), \quad (21)$$

where  $N_0$  is a minimum aggregation number,  $b_m$  is the sum of the coherent neutron scattering length of a monomer, and  $V_m$  is the volume of monomer in a particle.

When the total and free monomer molar concentrations are represented by  $C$  and  $C_1$ , respectively,

$$C - C_1 = \sum_{N=N_0}^{\infty} C_N, \quad (22)$$

$C_1$  can be equalized with the critical micelle concentration. Then the weight-average aggregation number  $\bar{N}$  is described as follows:

$$\bar{N} = \frac{\sum_{N=N_0}^{\infty} C_N N}{\sum_{N=N_0}^{\infty} C_N} = \frac{\sum_{N=N_0}^{\infty} C_N N}{C - C_1}. \quad (23)$$

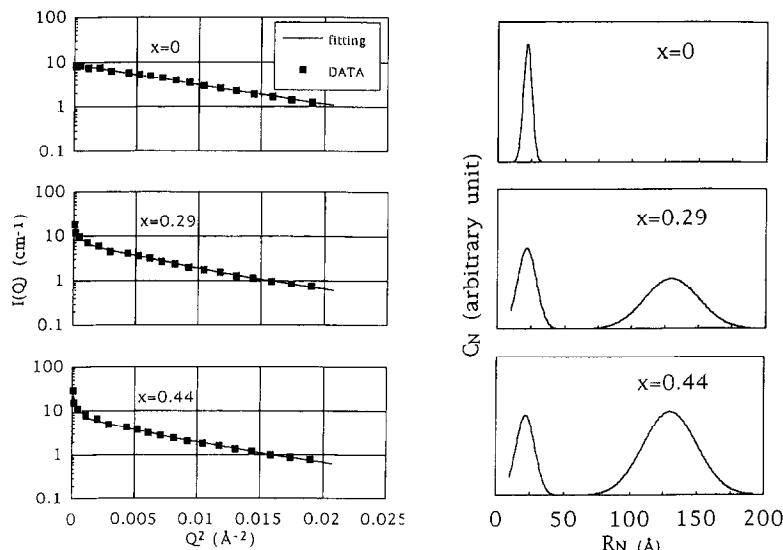


Fig. 10. Guinier plots of SANS for  $C_{12}$ DAO/hexanol/water mixtures and the size distribution of molecular assemblies.  $C_{12}$ DAO concentrations are 50 mM. Solid lines in Guinier plots represent the fitting curves for the theoretical analysis.

If particles are approximated as an equivalent sphere with radius  $R_N$ ,

$$R_{G,N}^2 = (3/5)R_N^2, \quad NV_m = (4/3)\pi R_N^3, \quad (24)$$

and

$$I(Q) = (b_m - \rho_s V_m)^2 \sum_{N=N_0}^{\infty} C_N N \exp(-R_N^2 Q^2/5). \quad (25)$$

When the set of  $C_N$  from  $C_{N_0}$  to  $C_{\infty}$  was selected for particles with radius  $R_N$  from  $R_{N_0}$  to  $R_{\infty}$ , the optimum set of  $C_N$  was determined by fitting the calculated  $I(Q)$  curve to the observed curve on the basis of Eqs. (22)–(25).  $C_N$  values as a function of  $R_N$  and the fitting curves are given in Fig. 10. The fitting curves satisfied the observed data.  $C_N$  values for  $C_{12}$ DAO/hexanol/water ternary systems displayed two maxima, that is, the distribution was bimodal. This is compared with the  $C_N$  curve for an aqueous  $C_{12}$ DAO solution without hexanol, which had a maximum at a certain  $R_N$  value.

While the concentration of particles with  $R_{\max} = 22 \text{ \AA}$  decreased with increased mixing fractions of hexanol, that with  $R_{\max} = 130 \text{ \AA}$  increased. Smaller particles are assigned to regular  $C_{12}$ DAO micelles. On the other hand, larger globular particles could be microemulsions which are hexanol droplets

stabilized by a shell of surfactant molecules. Fig. 11 shows a schematic representation of the coexistence of micelles and microemulsions. The particle diameters of 50–400  $\text{\AA}$  observed by TEM comprise the distribution of particle sizes evaluated from SANS. The numerical values of the hydrodynamic radius  $R_H$  evaluated from light scattering provided the average of the bimodal distribution, and naturally increased with the mixing fraction of hexanol.

Some workers have applied SANS analysis to polydisperse molecular assemblies. Kotlarchyk et al. [23] reported that the size polydispersity of

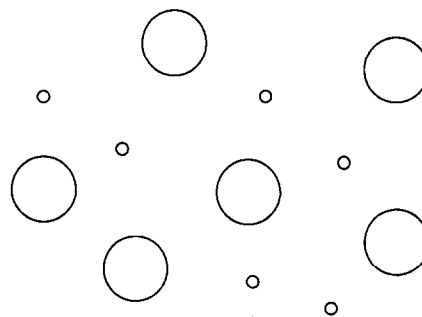


Fig. 11. Schematic representation of the coexistence of spherical micelles and microemulsions in 50 mM  $C_{12}$ DAO/20 mM hexanol/water ( $X = 0.29$ ) system.

the water core was appreciable in decane/AOT/water microemulsions. Lin et al. [29] evaluated the size distribution for polydisperse rodlike micelles formed by short-chain lecithin. These reports indicate that SANS is a beneficial method for characterizing polydispersity, as well as the structures of small particles such as ellipsoidal micelles and short distances such as the bilayer thickness. Israelachvili [72] predicted the possibility of the coexistence of microemulsion and micelles. Numerical analysis based on the theoretical aspect for polydisperse globular particles have confirmed that molecular assemblies in the  $L_1$  phase exhibit a bimodal distribution. However, no other SANS results for the component analysis in multimodal distributions have been reported, although such polydisperse systems are anticipated.

### Acknowledgments

This work was partly supported by Hayashi Memorial Foundation for Female Natural Scientists. Author is deeply indebted to Mr M. Kakitani, Mr H. Okamura, Professors M. Furusaka, K. Takagi, and Y. Sawaki for the SANS measurement and useful discussions.

### References

- [1] D.O. Shah and R.S. Schechter, Eds. *Improved Oil Recovery by Surfactant and Polymer Flooding*, Academic Press, New York, 1977.
- [2] P. Speiser, in: *Reverse Micelles*, Eds. P.L. Luisi and B.E. Straub, Plenum, New York, 1984.
- [3] D.O. Shah, Ed., *Macro and Microemulsions: Theory and Applications*, Am. Chem. Soc. Symp. Ser., 272, Washington, DC, 1985.
- [4] C.H. Chew and L.M. Gan, *J. Polym. Sci.*, 23 (1985) 225.
- [5] V. Chen, G.G. Warr, D.F. Evans and F.G. Prendergast, *J. Phys. Chem.*, 92 (1988) 768.
- [6] I.S. Barnes, S.T. Hyde, B.W. Ninham, P.-J. Derian, M. Drifford and T.N. Zemb, *J. Phys. Chem.*, 92 (1988) 2286.
- [7] W. Jahn and R. Strey, *J. Phys. Chem.*, 92 (1988) 2294.
- [8] B. Lindmann, K. Shinoda, M. Jonströmer and A. Shinohara, *J. Phys. Chem.*, 92 (1988) 4902.
- [9] U. Olsson, K. Nagai and H. Wennerström, *J. Phys. Chem.*, 92 (1988) 6675.
- [10] K. Chokski, S. Qutubuddin and A. Hussam, *J. Colloid Interface Sci.*, 129 (1989) 315.
- [11] M. Aoudia, M.A.J. Rodgers and W.H. Wade, *J. Colloid Interface Sci.*, 144, (1990) 353.
- [12] J.L. Green, *J. Phys. Chem.*, 94 (1990) 5647.
- [13] R. Strey, R. Schomäcker, D. Roux, F. Nallet and U. Olsson, *J. Chem. Soc. Faraday Trans.*, 86 (1990) 2253.
- [14] Y.J. Uang, T.D. Flaim and F.D. Blum, *J. Colloid Interface Sci.*, 139 (1990) 381.
- [15] P. Schurtenberger, L.J. Magid, S.M. King and P. Lindner, *J. Phys. Chem.*, 95 (1991) 4173.
- [16] K.-V. Shubert and R. Strey, *J. Chem. Phys.*, 95 (1991) 8532.
- [17] S.T. Hyde, B.W. Ninham and T. Zemb, *J. Phys. Chem.*, 93, (1983) 1464.
- [18] J.B. Hayter, Ber. Bunsenges. Phys. Chem., 85 (1981) 887; *Faraday Discuss. Chem. Soc.*, 76 (1983) 7.
- [19] J.B. Hayter and J. Penfold, *Molec. Phys.*, 42 (1981) 109; *Colloid Polym. Sci.*, 261 (1983) 1022.
- [20] J.B. Hayter and M. Zulauf, *Colloid Polym. Sci.*, 260 (1982) 1023.
- [21] J. Kalus, H. Hoffmann, K. Reizlein and W. Ulbricht, Ber. Bunsenges. Phys. Chem., 86 (1982) 37.
- [22] R. Triolo, L.J. Magid, J.S. Johnson Jr. and H.R. Child, *J. Phys. Chem.*, 86 (1982) 3689; R. Triolo, J.B. Hayter, L.J. Magid and J.S. Johnson Jr., *J. Chem. Phys.*, 79 (1983) 1977.
- [23] M. Kotlarchyk, S.-H. Chen and J.S. Huang, *J. Phys. Chem.*, 86 (1982) 3273.
- [24] L.J. Magid, K.A. Daus, P.D. Butler and R.B. Quincy, *J. Phys. Chem.*, 87 (1983) 5472.
- [25] D. Bendedouch and S.-H. Chen, *J. Phys. Chem.*, 87, (1983) 1653; D. Bendedouch, S.-H. Chen and W.C. Koehler, *J. Phys. Chem.*, 87 (1983) 2621.
- [26] M. Zulauf, K. Weckstrom, J.B. Hayter, V. Degiorgio and M. Corti, *J. Phys. Chem.*, 89 (1985) 3411.
- [27] F. Quirion and L.J. Magid, *J. Phys. Chem.*, 90 (1986) 5435.
- [28] E.Y. Sheu, S.H. Chen and J.S. Huang, *J. Phys. Chem.*, 91 (1987) 1535.
- [29] T.-L. Lin, S.-H. Chen, N.E. Gabriel and M.F. Roberts, *J. Phys. Chem.*, 91 (1987) 406.
- [30] V. Degiorgio, M. Corti and L. Cantu, *Chem. Phys. Lett.*, 151, (1988) 349; V. Degiorgio, M. Corti, R. Piazza, L. Cantu and A.R. Rennie, *Colloid Polym. Sci.*, 269 (1991) 501.
- [31] K.S. Rao, P.S. Goyal, B.A. Dasannacharya, V.K. Kelker, C. Manohar and S.V.G. Manon, *Pramana*, 37 (1991) 31.
- [32] P.S. Goyal, S.V.G. Manon, B.A. Dasannacharya and V. Rayagoparan, *Chem. Phys. Lett.*, 211 (1993) 559.
- [33] H. Pilsl, H. Hoffmann, S. Hofmann, J. Kalus, A.W. Kencone, P. Linder and W. Ulbricht, *J. Phys. Chem.*, 97 (1993) 2754.
- [34] B. Cabane, R. Duplessix and T. Zemb, in: *Surfactants in Solution*, eds. K.L. Mittal and B. Lindman, 1 (1984) 373; B. Cabane, R. Duplessix and T. Zemb, *J. Physique*, 46 (1985) 2161.
- [35] E.Y. Sheu and S.H. Chen, *J. Phys. Chem.*, 92 (1988) 4466.

- [36] J.-P. Hansen and J.B. Hayter, *Molec. Phys.*, 46 (1982) 651.
- [37] S. Ikeda, M. Tsunoda and H. Maeda, *J. Colloid Interface Sci.*, 70 (1979) 448.
- [38] T. Imae and S. Ikeda, *Colloid Polym. Sci.*, 263 (1985) 756.
- [39] T. Imae, M. Sasaki and S. Ikeda, *J. Colloid Interface Sci.*, 131 (1989) 601.
- [40] T. Imae, *J. Phys. Chem.*, 94 (1990) 5953.
- [41] K. Hashimoto and T. Imae, *Langmuir*, 7 (1991) 1734.
- [42] T. Imae and B. Trend, *J. Colloid Interface Sci.*, 145 (1991) 207.
- [43] T. Imae and T. Iwamoto, *J. Colloid Interface Sci.*, 152 (1991) 289.
- [44] T. Imae, *J. Jpn. Oil Chem. Soc.*, 41 (1992) 616.
- [45] T. Imae and N. Hayashi, *Langmuir*, 9 (1993) 3385.
- [46] A. Guinier and G. Fournet, *Small-Angle Scattering of X-rays*, Wiley, New York, 1955; O. Glatter and O. Kratky, *Small Angle X-ray Scattering*, Academic Press, London, 1982; L.A. Feigin and D.I. Svergun, *Structure Analysis by Small-Angle X-ray and Neutron Scattering*, Ed. G.W. Taylor, Plenum, New York, 1987; P. Lindner and Th. Zemb, *Neutron, X-ray and Light Scattering: Introduction to an Investigative Tool for Colloidal and Polymeric Systems*, North-Holland, Amsterdam, 1991.
- [47] S.H. Chen, *Ann. Rev. Phys. Chem.*, 37 (1986) 351; S.H. Chen and T.L. Lin, *Meth. Exp. Phys.*, 23 (1987) 489.
- [48] P. Schurtenberger, L.J. Magid, S.M. King and P.J. Lindner, *J. Phys. Chem.*, 95 (1991) 4173.
- [49] J.P. Hansen and I.R. McDonald, *Theory of Simple Liquids*, Academic Press, London, 1976.
- [50] R. Strey, R. Schomacker, D. Roux, F. Nallet and U. Olsson, *J. Chem. Soc., Faraday Trans.*, 86 (1990) 2253.
- [51] J.G. Weers, K.F. Rathman and D.R. Scheuing, *Colloid Polym. Sci.*, 268 (1990) 832.
- [52] M.S. Bakshi, R. Crisantino, R. De Lisi and S. Milioto, *J. Phys. Chem.*, 97 (1993) 6914.
- [53] S. Hofmann, A. Rauscher and H. Hoffmann, *Ber. Bunsenges. Phys. Chem.*, 95 (1991) 153.
- [54] C. Tanford, *The Hydrophobic Effect*, Wiley, New York, 1973.
- [55] T. Imae and M. Kakitani, unpublished work.
- [56] E.J.W. Verwey and J.Th.G. Overbeek, *Theory of the Stability of Lyophobic Colloids*, Elsevier, Amsterdam, 1948.
- [57] J.B. Hayter, *Langmuir*, 8 (1992) 2873.
- [58] N. Gorski, M. Gradzielski and H. Hoffmann, *Langmuir*, 10 (1994) 2594.
- [59] K. Takagi, B.R. Suddaby, S.L. Vadas, C.A. Backer and D.G. Whitten, *J. Am. Chem. Soc.*, 108 (1986) 7865.
- [60] K. Takagi, H. Fukaya, N. Miyake and Y. Sawaki, *Chem. Lett.*, (1988) 1053.
- [61] K. Takagi, E. Nambara, H. Usami, M. Itoh and Y. Sawaki, *J. Chem. Soc., Perkin Trans. I*, (1991) 655.
- [62] K. Takagi, M. Itoh, H. Usami, T. Imae and Y. Sawaki, *J. Chem. Soc. Perkin Trans. II*, (1994) 1003.
- [63] T. Wolff and N. Muller, *J. Photochem.*, 23 (1983) 131: 22 (1983) 61.
- [64] K. Takagi, N. Miyake, E. Nakamura, H. Usami and Y. Sawaki, *J. Chem. Soc., Faraday Trans. I*, 84 (1988) 3475.
- [65] A. Ueno, F. Moriwaki, Y. Iwama, I. Suzuki, T. Osa, T. Ohta and S. Nozoe, *J. Am. Chem. Soc.*, 113 (1991) 7034.
- [66] H. Okamura, T. Imae and M. Furusaka, *J. Colloid Interface Sci.*, 168 (1994) 217.
- [67] T. Imae, T. Tsubota, H. Okamura, O. Mori, K. Takagi, M. Itoh and Y. Sawaki, *J. Phys. Chem.*, 99 (1995) 6046.
- [68] T. Imae, O. Mori, K. Takagi, M. Itoh and Y. Sawaki, *Colloid Polym. Sci.*, 273 (1995) 579.
- [69] G. Platz, G. Thunig and H. Hoffmann, *Ber. Bunsenges. Phys. Chem.*, 96 (1992) 667.
- [70] T. Imae, T. Iwamoto, G. Platz, C. Thunig, *Colloid Polym. Sci.* 272, (1994) 604.
- [71] H. Okamura, T. Imae, K. Takagi, Y. Sawaki and M. Furusaka, *J. Colloid Interface Sci.*, in press.
- [72] J.N. Israelachvili, *J. Chem. Soc., Faraday Trans. II*, 72 (1976) 1525.